Journal of Structural Geology 30 (2008) 1034–1046

Contents lists available at ScienceDirect

Journal of Structural Geology

journal homepage: www.elsevier.com/locate/jsg

Recognizing the seismic cycle along ancient faults: CO_2-induced fluidization of breccias in the footwall of a sealing low-angle normal fault

S.A.F. Smith [a,*], C. Collettini [b], R.E. Holdsworth [a]

[a] Reactivation Research Group, Department of Earth Sciences, University of Durham, Durham, DH1 3LE, UK
[b] Geologia Strutturale e Geofisica, Dipartimento Di Scienze della Terra, Universita degli studi di Perugia, Perugia, 06123, Italy

ARTICLE INFO

Article history:
Received 26 September 2007
Received in revised form 10 April 2008
Accepted 28 April 2008
Available online 10 May 2008

Keywords:
Breccia
Fluidization
Interseismic
Fault-valve
Low-angle normal fault

ABSTRACT

The Zuccale low-angle normal fault exposed on the island of Elba, Italy, is a crustal-scale structure which contains a strongly foliated fault core. In the immediate footwall of the Zuccale fault, cohesive fault-related breccias which were initially deformed by typical frictional deformation mechanisms experienced fluidization over areas of at least 10^{-2}–10^{-3} km^2.

Three internal variants of fluidized breccia are recognized, with each related to a separate fluidization event. Characteristics of the fluidized breccias include: (1) a highly irregular 'intrusive' boundary with the overlying fault core; (2) no grain-scale evidence for typical frictional deformation mechanisms; (3) an association with carbonate cements indicating that fluids contained CO_2; and (4) a clast-preferred orientation suggesting that fluids were moving vertically and spreading laterally as they encountered the foliated fault core.

Our observations suggest that the fluidized breccias are representative of the interseismic period along the Zuccale low-angle fault, and developed across small fault patches during build-ups in fluid overpressure. Attainment of a critical fluid overpressure triggered embrittlement and the formation of low-angle slip surfaces and sub-vertical tensile veins within the overlying fault core, which may account for the presence and the dimensions (10^{-1}–10^{-3} km^2) of rupture surfaces which produce microseismicity along active low-angle normal faults in central Italy.

1. Introduction

Fluids exert a fundamental control on the mechanical and chemical behaviour of all types of fault and shear zone. There is a voluminous literature detailing field, laboratory and theoretical work carried out in an attempt to understand the role of fluids in earthquake rupture, the formation of hydrothermal ore deposits, and the long-term evolution of faulted regions of the crust and lithosphere at all depths and scales (e.g. reviews by Hickman et al., 1995; Oliver, 1996; Sibson, 2000; Person et al., 2007). Increasingly it is recognized that cycling of fluid pressure, e.g. 'fault-valve' models (Sibson, 1990), within faults and shear zones strongly affects their mechanical behaviour, and can be intimately linked to the earthquake cycle (e.g. Parry and Bruhn, 1990; Sibson, 1992, 2007; Cox, 1995; Henderson and McCaig, 1996; Nguyen et al., 1998; Famin et al., 2005).

Low-angle normal faults, which dip less than 30°, have received considerable attention since standard 'Andersonian' frictional fault theory does not predict such orientations and because large earthquakes on low-angle normal faults are rare or absent (Anderson, 1942; Jackson and White, 1989; Wernicke, 1995; Collettini and Sibson, 2001; Axen, 2004, 2007). Low-angle normal faults may slip over prolonged periods of time if fault rock materials lining the fault surface possess a low friction coefficient (e.g. Numelin et al., 2007), or if high fluid pressures are generated within, or adjacent to, the fault zone (e.g. Axen, 1992). Attainment of tensile fluid overpressure ($P_f > \sigma_3$) is critical for reactivation and slip along low-angle normal faults, particularly in the upper 10 km of the brittle crust. For example, Collettini and Barchi (2002) applied frictional reactivation theory to study the conditions necessary for reactivation of the Altotiberina fault, an active low-angle normal fault in central Italy. They found that the Altotiberina fault can be reactivated for low values of differential stress ($\sigma_1 - \sigma_3 < 28$ MPa), relatively high values of tensile strength of the surrounding rocks ($\sim$10 MPa), and tensile fluid overpressure $P_f > \sigma_3$ (e.g. $\lambda_v > 0.93$). There is strong evidence from the footwalls of metamorphic core complexes and their associated low-angle normal faults, where vein and fracture networks are commonly observed, that tensile fluid overpressure is locally obtained (e.g. Reynolds and Lister, 1987). However, the factors leading to focused

* Corresponding author: Tel. +44 (0)798 8777642; fax: +44 0191 3342301.
E-mail addresses: steven.smith@durham.ac.uk (S.A.F. Smith), colle@unipg.it (C. Collettini), r.e.holdsworth@durham.ac.uk (R.E. Holdsworth).

0191-8141/$ – see front matter © 2008 Elsevier Ltd. All rights reserved.
doi:10.1016/j.jsg.2008.04.010

fluid flow and to the development of fluid overpressure at specific sites are unknown, and there is still a paucity of direct geological evidence for any form of fluid cycling along low-angle normal faults.

The aim of this paper is to describe in detail the geological setting, microstructural characteristics, and evolution of a suite of frictional fault rocks (breccias) which we believe to have experienced widespread fluidization beneath the Zuccale fault, a low-angle normal fault exposed on the Island of Elba. We focus our attention on a single coastal outcrop which contains 100% exposure in the immediate footwall of the Zuccale fault, and use our observations to develop a conceptual model for fluidization. We discuss our observations in the context of fluid cycling, the development of fluid overpressure associated with low-angle normal faults, and the recognition of fault rocks which represent particular phases of the seismic cycle.

2. Geological context

2.1. The northern Apennines

Elba lies ~20 km to the west of Tuscany in the northern Tyrrhenian Sea. This area has experienced two contrasting phases of deformation, both of which migrated progressively from west to east (Fig. 1a; Elter et al., 1975; Pauselli et al., 2006). An earlier phase of Cretaceous to Quaternary collision was followed by a later phase of Miocene to currently active post-collisional extension. Geological and geophysical studies have highlighted that a majority of post-collisional extension has been accommodated along shallowly east-dipping low-angle normal faults (Fig. 1a; Barchi et al., 1998; Jolivet et al., 1998; Pauselli et al., 2006; Collettini et al., 2006b; Chiaraluce et al., 2007). Active extension presently occurs along the Altotiberina low-angle normal fault, which produces abundant microseismicity ($M < 2.3$) at a rate of ~8.1 events day^{-1} km^{-2} (Chiaraluce et al., 2007) over a depth range of 4–14 km (Fig. 1a; Boncio et al., 1998, 2000). Microseismic activity occurs on rupture surfaces in the size range of 10^{-1}–10^{-3} km^2 (Sibson, 1989; Collettini and Barchi, 2002; Chiaraluce et al., 2007). The active regional stress field in central Italy is characterized by a sub-vertical σ_1 and an east–west to NE–SW trending, sub-horizontal σ_3 (Montone et al., 2004). Older, inactive low-angle normal faults are exhumed in western Tuscany and the Tyrrhenian islands, which includes the Zuccale fault exposed on Elba.

Central Italy is characterized by an anomalously high flux of non-volcanic CO_2, focused specifically within the area which has experienced widespread post-collisional extension (Fig. 1a; Chiodini et al., 2004). The flux of CO_2 reaches ~0.8 tonnes day^{-1} km^{-2}, whereas to the east of the active extensional front, the flux of CO_2 decreases rapidly. Based mainly on $^3He/^4He$ and $\delta^{13}C$ isotopic analysis, it appears that around 40% of the CO_2 gas discharged in central Italy is derived from the upper mantle, which acts as an important source of CO_2-bearing fluid to the base of the brittle crust (Chiodini et al., 2004; Minissale et al., 2000; Minissale, 2004). Two deep boreholes (Santo Donato at 4750 m below sea level and Santo Stefano at 3700 m below sea level) which penetrated the active Altotiberina fault encountered fluid overpressures which were ~85% of the lithostatic load ($\lambda_v = 0.85$), induced by trapped CO_2-bearing hydrous fluids in the footwall of the fault (Chiodini and Cioni, 1989). Several authors have suggested that deeply derived CO_2-bearing fluids play a critical role in the nucleation of crustal earthquakes and the time–space evolution of aftershocks in central Italy (e.g. Collettini and Barchi, 2002; Miller et al., 2004; Chiaraluce et al., 2007).

2.2. The Zuccale fault on the island of Elba

Elba consists of a series of 5 stacked thrust sheets (Complexes I–V) which formed during late Cretaceous–early Miocene shortening (Fig. 1b). All of the thrust sheets currently dip moderately to the west and are crosscut and displaced by the shallowly east-dipping Zuccale fault (Fig. 1b; Trevisan et al., 1967; Keller and Pialli, 1990; Bortolotti et al., 2001). Shear sense along the Zuccale fault is

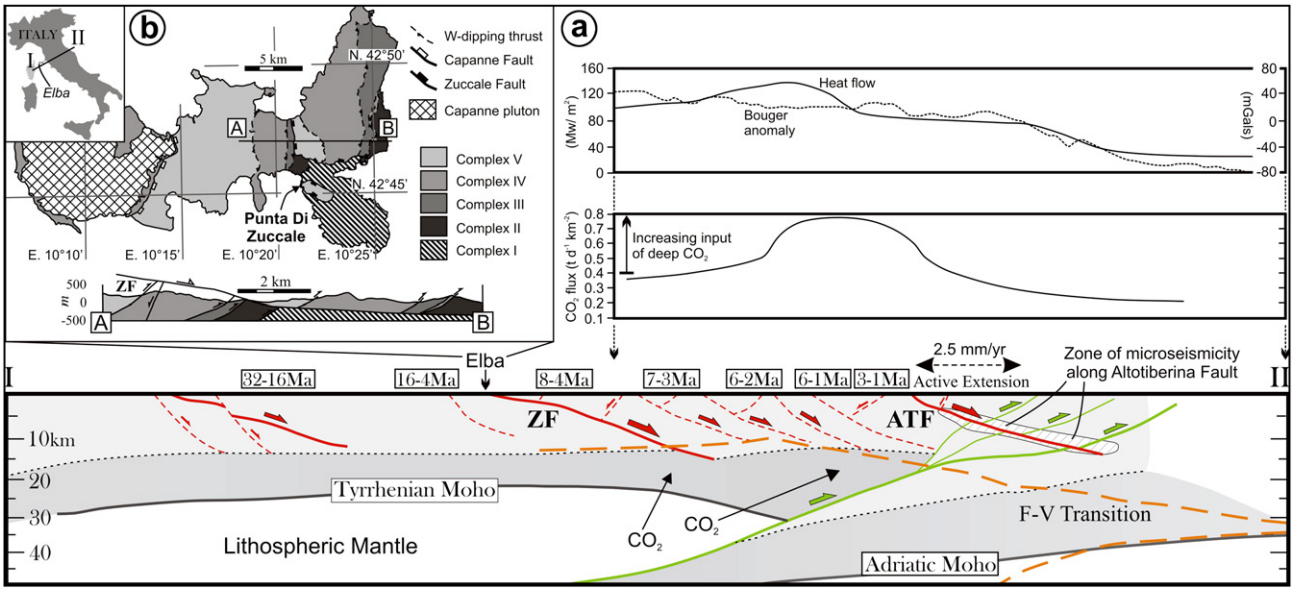

Fig. 1. (a) Crustal-scale cross section from Corsica to the Adriatic coast based partly on the CROP03 deep seismic reflection profile (Barchi et al., 1998). Location of the cross section is shown in part (b). The age ranges of syn-tectonic extensional basins are shown in white boxes. Extensional processes in the Tyrrhenian Sea and Tuscany have caused high average heat flows, a regional positive Bouger gravity anomaly, and a shallow Moho (after Collettini et al., 2006b). Additionally, the area is associated with high fluxes of deeply-derived CO_2. Location of the frictional–viscous (F–V) transition after Pauselli and Federico (2002). Zone of microseismicity along the Altotiberina Fault (ATF) after Chiaraluce et al. (2007). ZF, Zuccale fault. (b) Simplified geological map of Elba (after Trevisan et al., 1967) and cross section through central and eastern Elba highlighting the geometry of the Zuccale fault. Complex I, Paleozoic basement schists; Complex II, Tuscan metamorphic sequence; Complex III, Tuscan limestone sequence; Complex IV, Ligurian ophiolite sequence; Complex V, Cretaceous flysch.

uniformly top-to-the-east, and overall extensional offsets are c. 6–8 km (Keller and Coward, 1996). The movement history of the Zuccale fault is poorly constrained, but a majority of displacement is likely to have occurred between ~8 Ma and ~4 Ma based on ages obtained for displaced granitic intrusions (Dini et al., 2002), and for sediments deposited in extensional basins to the east (Pascucci et al., 1999). Extension on Elba was accompanied by intrusion of the Capanne (c. 6.9 Ma) and Porto Azzurro (c. 5.9 Ma) plutons, both of which were associated with significant hydrothermal fluid flow systems (Taylor and Turi, 1979; Dini et al., 2002; Maineri et al., 2003; Gagnevin et al., 2004; Rossetti et al., 2007).

The Zuccale fault is exposed particularly well at its type locality at Punta Di Zuccale (Fig. 1b), where it juxtaposes a hangingwall of Cretaceous sandstone and siltstone flysch deposits (Complex V) against a footwall of Palaeozoic quartzites and quartz–mica schists (Complex I; Fig. 2). Collettini and Holdsworth (2004) and Smith et al. (2007) studied the fault rock sequence and internal structure of the Zuccale fault, and only a brief summary of necessary details is provided below.

From bottom to top, the sequence of fault rocks found along the Zuccale fault consists of five units: (1) breccias and cataclasites derived exclusively from the Palaeozoic footwall rocks and containing clasts of quartzite and quartz–mica schist surrounded by a carbonate–chlorite–quartz matrix. These were deformed by frictional deformation mechanisms including fracture, grain fragmentation and grain rolling. Although their distribution is heterogeneous, they typically have a minimum thickness of ~3 m. Below, we refer to them as *frictional breccias*; (2) calc-mylonites and chlorite–talc–phyllonites; (3) foliated serpentinite with inclusions of tremolite–talc–chlorite schist; (4) carbonate-rich foliated cataclasites containing lenses of serpentinite, phyllonite, and calc–mylonite; (5) coarse fault breccias and foliated fault gouges derived predominantly from the hangingwall Cretaceous sandstones and siltstones. Throughout this paper we refer to fault rock units 2–5 as the 'fault core'. The footwall and fault core are crosscut by abundant carbonate veins, often possessing crack-seal textures, and interpreted to represent hydrofractures formed due to periodic build-ups in fluid overpressure (Collettini et al., 2006a). The largest hydrofracture veins link directly downwards into subsidiary, steeply-dipping extensional faults present in the footwall of the Zuccale fault (Fig. 2), strongly suggesting that these footwall faults focused and channelled fluid flow (Smith et al., 2007). Along part of the north south (transport-perpendicular) coastal section at Punta Di Zuccale, frictional breccias (fault rock unit 1) locally adopt a different, and unusual, appearance. Typically, these unusual breccias are grey to milky-white in colour and below we refer to them collectively as *grey breccias*.

3. Grey breccias

3.1. Field relationships

Grey breccias occur in the immediate footwall of the Zuccale fault where they occupy a minimum area in plan view of ~70 × 40 m, and occur over large areas of continuous outcrop and as a series of isolated windows which are eroded through the overlying fault rocks (Figs. 3–5). The total vertical extent of the grey breccias is unknown, but they are present to a depth of at least 3 m in the footwall of the Zuccale fault. Three internal variants of grey breccia are recognized and we refer to these as breccias A, B, and C

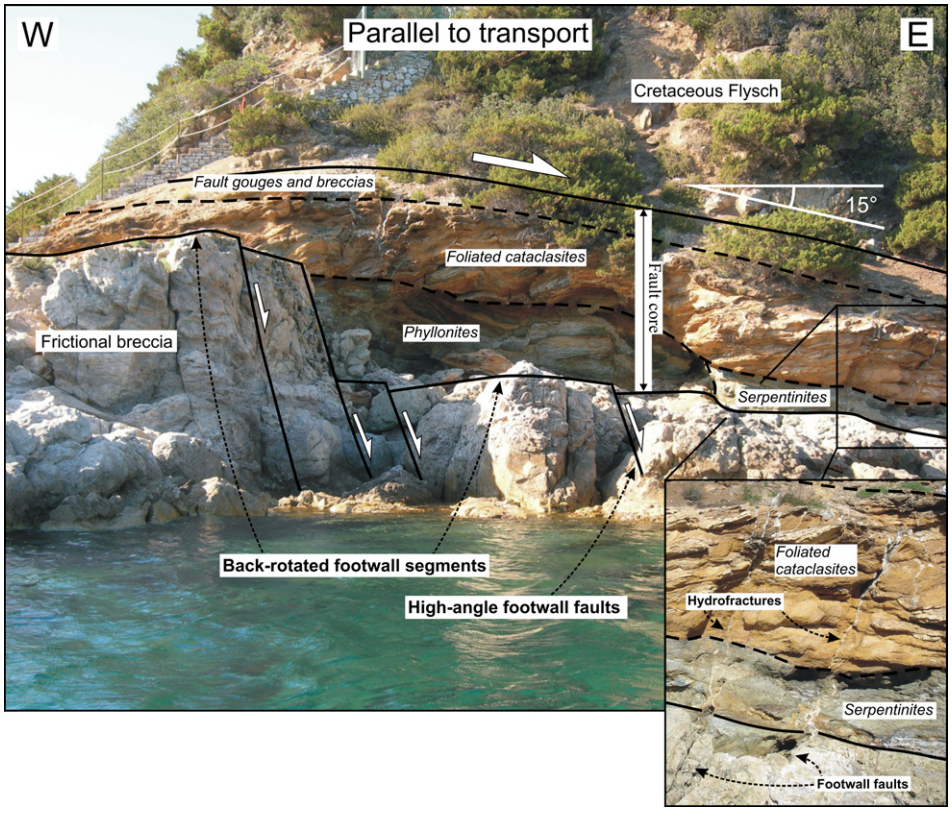

Fig. 2. Characteristic geometry of the Zuccale fault observed along an east–west coastal section at Punta Di Zuccale, where it places Cretaceous flysch in the hangingwall against Paleozoic schists in the footwall. Double headed arrow labelled 'Fault Core' is 5 m in thickness. Overall, the Zuccale fault dips ~15°E, but locally the base of the fault core has been back-rotated by a series of high-angle footwall faults, which also strongly control the distribution of individual fault rock units. Hydrofracture veins cross-cut the footwall and fault core, and are always directly linked to high-angle footwall faults (see inset photograph).

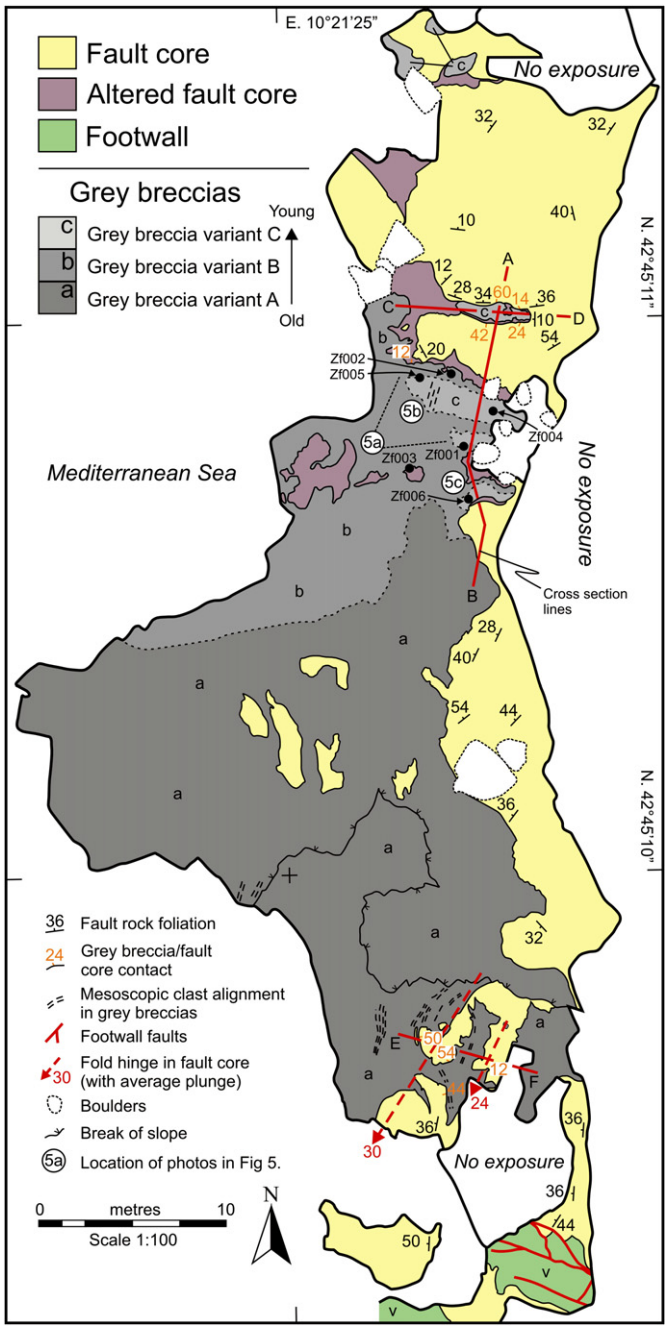

Fig. 3. Detailed geological map of the north–south coastal section at Punta Di Zuccale where grey breccias are present. Also shown are the cross section lines in Fig. 4, the locations of photographs in Fig. 5, and the locations of samples Zf001–Zf006 discussed in Section 4.2.

(Figs. 3, 4). They are differentiated in the field on the basis of colour, structural position beneath the Zuccale fault, textural features, and maximum clast size.

Grey breccia A is the most voluminous variant and occupies an area of ~40 × 40 m in the southern half of the mapped outcrop (Fig. 3). Compositionally and texturally it is highly heterogeneous, and is dominated by large blocks of basement quartzite and quartz–mica schist which can be up to several meters in diameter. The lithologies of clasts within this variant, and those in variants B and C, are indistinguishable from the local wallrock.

Variants B and C are texturally much more homogenous. Both are grey to milky-white in colour, and contain clasts of basement quartzite and quartz–mica schist not exceeding several tens of centimetres in diameter. Breccia C is differentiated from B on the basis of two specific mesoscopic characteristics. First, it occurs solely as discrete pods of material which sit at topographically and structurally higher levels than B (Figs. 4, 5a). Second, breccia C possesses a distinct honeycomb weathering texture, particularly noticeable towards its base, which appears to reflect erosion and removal of large clasts (Fig. 5b).

The three variants of grey breccia appear to have formed at different times based on their structural relationship to extensional slip surfaces within the overlying foliated core of the Zuccale fault. Slip surfaces are commonly highly polished and associated with a thin (<1 mm) veneer of ultra-fine grained cataclastic material. Breccia A appears to be the oldest variant, because in places the upper surface of this breccia is defined by a cross-cutting extensional slip surface which contains well-developed east–west slickenlines. In turn, breccias B and C cross-cut the same slip surface and so, by definition, must be younger than A. Breccia C is interpreted to be younger than B because of its occurrence as isolated pods of material which sit on top of and appear to originate from within B (Figs. 4, 5a).

Importantly, there is strong evidence that the coastal section containing the grey breccias is underlain by a major north–south trending high-angle extensional fault like those described in Section 2.2 and shown in Fig. 2. Smith et al. (2007) showed that well-exposed footwall faults are directly associated with (Fig. 2): (1) the preservation of phyllonitic fault rocks as isolated lenses of material; (2) inclined flow folds within the fault core; and (3) back-rotation of footwall blocks so that locally they are sub-horizontal or dip westward. All of these structural relations are found in the area containing the grey breccias (Fig. 3). Large flow folds are present within the fault core in the southern half of the mapped outcrop, and all fault core rocks dip moderately to the west or north-west, indicating that the fault core has experienced local back-rotation.

3.2. The boundary between the grey breccias and the overlying fault core

All three variants of grey breccia appear to preserve 'intrusive' relationships with overlying foliated fault rocks within the core of the Zuccale fault (Figs. 4, 5, 7b). The boundary between the grey breccias and the overlying fault core is well defined and typically has a highly irregular nature, preserving undulations with wavelengths between 10 cm and 5 m, both parallel and perpendicular to the easterly transport direction within the Zuccale fault. These undulations are directly associated with warping and folding of the overlying fault core, so that the foliation within the overlying fault rocks closely follows the shape of the underlying boundary (Fig. 4). In detail, the boundary has a cuspate-lobate nature (Fig. 5c). Additionally, small fragments (<30 cm in diameter) of heavily altered fault core material are commonly found 'floating' within the underlying grey breccias (Fig. 5c). Within breccia variants A and C a mesoscopic north–south alignment of elongate clasts of quartzite and quartz–mica schist can be observed on sub-horizontal (plan view) surfaces (Fig. 6).

3.3. Microstructural observations

Frictional breccias are typically characterized by a mosaic texture (following the terminology of Mort and Woodcock, 2008), so that at any scale of observation, the textural framework appears to be 'clast-supported' (Fig. 7a). The frictional breccias contain abundant cataclastic fractures which are commonly lined with fibrous chlorite. The matrix of the frictional breccias typically consists of fine-grained quartz, chlorite and sericite, derived from

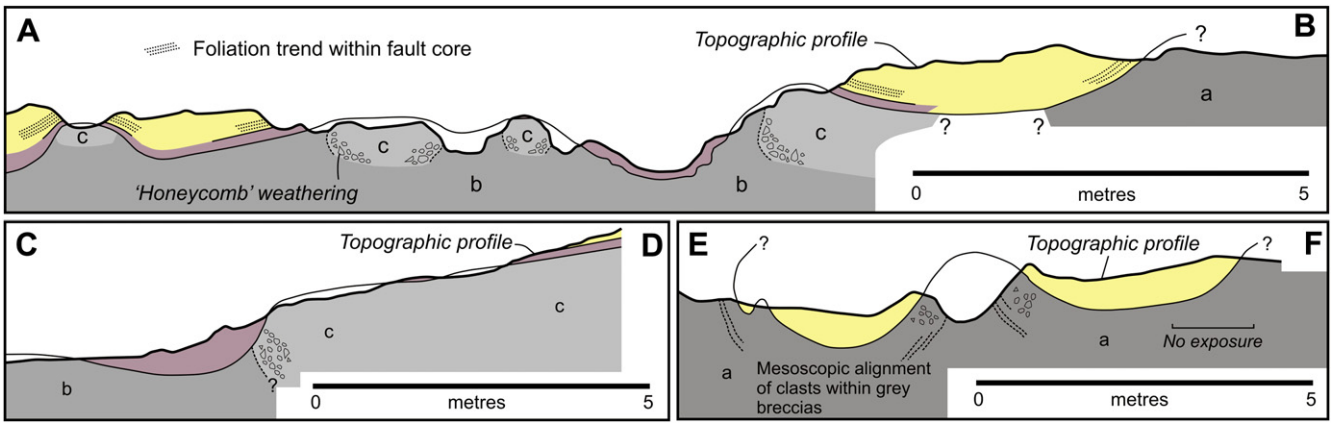

Fig. 4. Cross sections through the grey breccias and overlying fault rocks within the core of the Zuccale fault. Key is the same as Fig. 3. Note the presence of a mesoscopic clast alignment within the grey breccias, and a layer of altered fault core overlying the grey breccias.

comminution of larger clasts. Qualitatively, clasts within the frictional breccias at any scale of observation have an angular to sub-angular appearance, and contain no visible shape-preferred orientation (Fig. 7a). They appear relatively fresh and have not been overgrown by any late alteration or replacement products.

Grey breccias appear remarkably different on a grain-scale, and their overall texture does not readily fit into one of the breccia classes proposed by Mort and Woodcock (2008); (Fig. 7b). At any scale of observation, the breccia framework appears to be 'matrix-supported'. Relatively large clasts of quartzite and quartz–mica schist (up to ~1000 μm) are isolated within an ultra-fine grained matrix. There is a complete lack of any localized deformation features such as cataclastic fractures or shear bands. Qualitatively, clasts within the grey breccias have a sub-rounded to rounded appearance and are commonly overgrown by euhedral crystals of colourless dolomite (Fig. 8a). In thin section, the boundary between the grey breccias and the overlying fault core preserves a well-defined, irregular nature (Fig. 8b). Immediately above the boundary, in a layer 30 cm to 1 m thick, the fault core is highly altered and is dominated by fine-grained Fe-oxide phases and inter-grown calcite and dolomite crystals (Figs. 3, 4, 5, 8b). These carbonate crystals are fresh and undeformed, and often preserve primary growth zoning (Fig. 8c). In places, a relict breccia texture is overgrown by undeformed, subhedral–anhedral calcite crystals (Fig. 8d). Table 1 provides a summary of microstructural observations of frictional breccias and grey breccias.

4. Quantifying grain-scale deformation in the grey breccias

4.1. Analysis of fragmented counterparts

Monzawa and Otsuki (2003) and Otsuki et al. (2003) proposed a quantitative method to determine whether a particular granular fault rock has experienced fluidization. The key parameter analyzed using their method is the 'detection probability of fragmented counterparts' in thin sections of fault rock. A clast in thin section is considered a fragmented counterpart when it can be recognized that it was originally part of a larger clast. In other words, if two clast fragments are found adjacent to one another, and they evidently fit together like a jigsaw puzzle, they can be considered fragmented counterparts.

During frictional deformation, granular fault rocks such as breccias and cataclasites, which consist of packed and interlocking clasts, experience continuous fracturing due to high stresses at grain–grain contacts. Consequently, the probability that clasts will be fractured during frictional deformation is high.

Once a granular fault rock becomes fluidized, the only mechanism capable of generating new clast fragments is head-on collision between clasts, or between clasts and the wall rocks. However, Monzawa and Otsuki (2003) showed that in most circumstances the probability of fragmenting clasts smaller than a few millimetres during fluidization is virtually zero, because the collision velocities required are extremely high (e.g. 10 m s^{-1} for clasts of quartzite 1 mm in diameter). Although only currently developed for 2-dimensional analysis, their simple theoretical treatment indicates that an assessment of the number of fragmented counterparts can yield important insights into whether a granular fault rock has experienced fluidization or not.

The analysis of fragmented counterparts involves scanning thin sections under the optical microscope and searching for fragmented counterparts with radius $r < r < r + \Delta r$ within a given area for a given magnification. During fault slip, fragmented counterparts will move away from one another. The total number of identifiable fragmented counterparts with radius r, $\Delta N_f(r)$, can be expressed as a percentage probability, $P(r)$, relative to the total number of clasts with radius r, $\Delta N_t(r)$. At this stage we define the parameter $R_f(r)$ as the fragmentation rate per clast per unit incremental fault slip, Δs. Therefore, the total number of fragmented counterparts produced during incremental fault slip is $N_t(r)R_f(r)\Delta s$. For a fragmented counterpart to remain identifiable, it must stay within a critical distance, d_c. The probability at which a pair of counterparts can be identified after fragmentation is proportional to $(d_c/v_r)/\Delta s$, where v_r is the mean residence 'time' for counterparts to stay within d_c. In summary, Monzawa and Otsuki (2003) show that the total number of identifiable fragmented counterparts is proportional to $N_t(r)R_f(r)\Delta s \times d_c/v_r\Delta s$, and the detection probability of fragmented counterparts is:

$$P(r) \equiv \frac{N_f(r)}{N_t(r)} \propto \frac{R_f(r)d_c}{v_r} \quad (1)$$

As noted above, $R_f(r)$ during fluidization is likely to be low, whereas in the frictional regime, it can be high due to grain–grain contact stresses. Additionally, v_r is likely to be considerably higher for the fluidization regime compared to the frictional regime because clasts are able to move more freely in a fluid phase. Consequently, $P(r)$ is expected to be small for fluidized fault rocks, but much larger for fault rocks produced during typical frictional deformation.

We measured $P(r)$ in 8 thin sections of breccia from the immediate footwall of the Zuccale fault (Fig. 9). Four thin sections were cut from 2 samples of breccia deformed by typical frictional mechanisms (PZ019, PZ020), and 4 thin sections were cut from 2

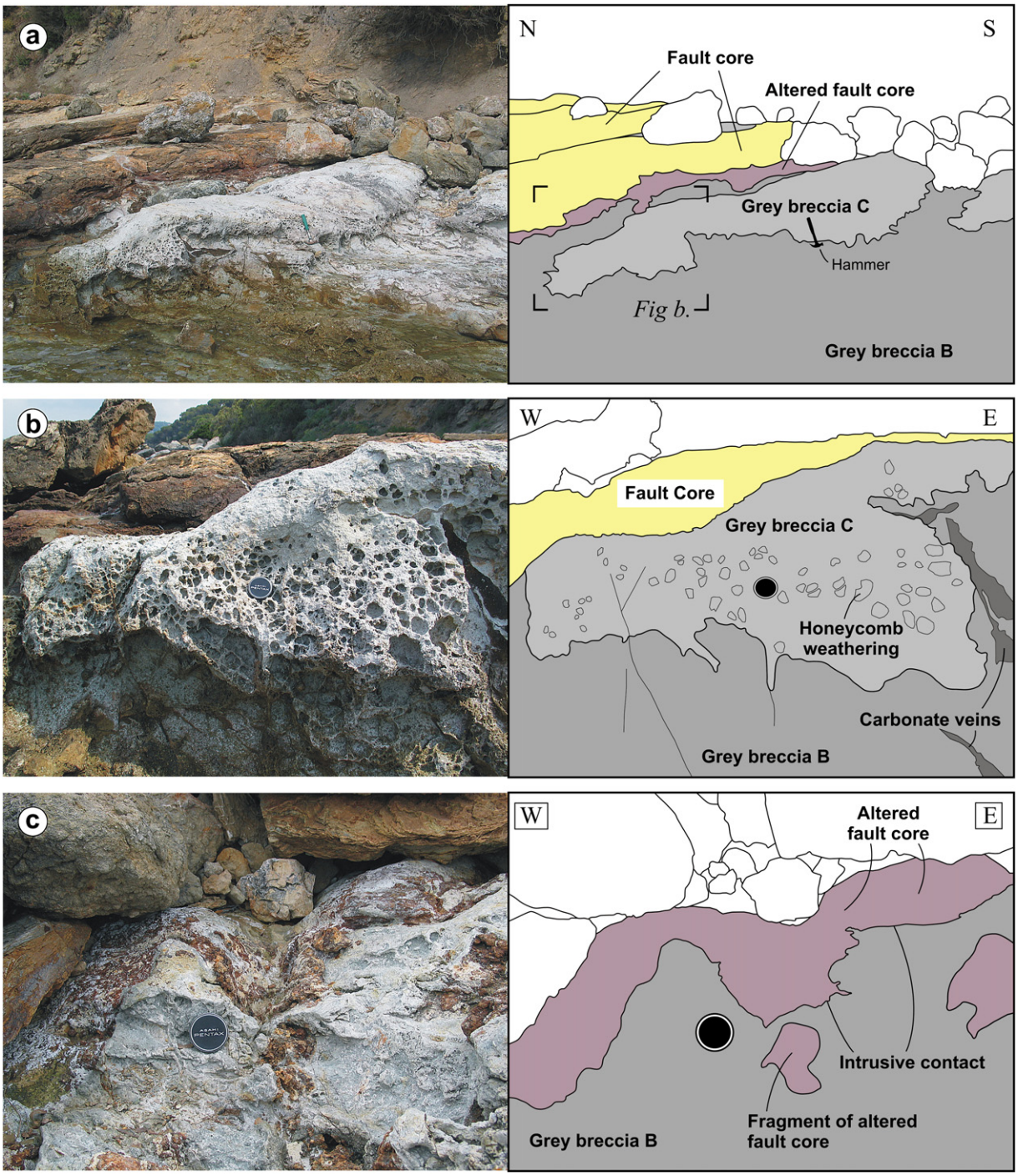

Fig. 5. Photographs and detailed sketches of the grey breccias and overlying fault core. Locations of photographs are shown in Fig. 3.

samples of grey breccia (PZ001 from variant C, PZ003 from variant B). Fragmented counterparts were analyzed over the size range 10–4000 μm, and 200–600 measurements were carried out on each thin section.

The *P* values of sample PZ020 are the highest, and reach 60–70% for clast diameters of ~1000 μm, decreasing to <50% at clast diameters of <100 μm. The average *P* value for this sample is 61%. Sample PZ019 also shows high values, with an average of 44.5%. Again, *P* values reach 50–70% for clast diameters of ~1000 μm, decreasing to <40% for clast diameters of <100 μm. In both cases, *P* clearly shows a strong clast size dependency. This is related to the fact that the tensile strength of clasts is strongly size dependent, and consequently the fragmentation rate $R_f(r)$ is also size dependent (Monzawa and Otsuki, 2003; Otsuki et al., 2003). This highlights the fact that when carrying out fragmented counterpart analysis it is necessary to consider clast sizes over as wide a size range as possible.

In marked contrast, samples PZ001 and PZ003 show uniformly low *P* values and no obvious size dependency. The average values of *P* are 8% for PZ001 and 7.6% for PZ003. There are clearly 2 separate groups identifiable in our results, the first group consisting of PZ019 and PZ020, the second group consisting of PZ001 and PZ003.

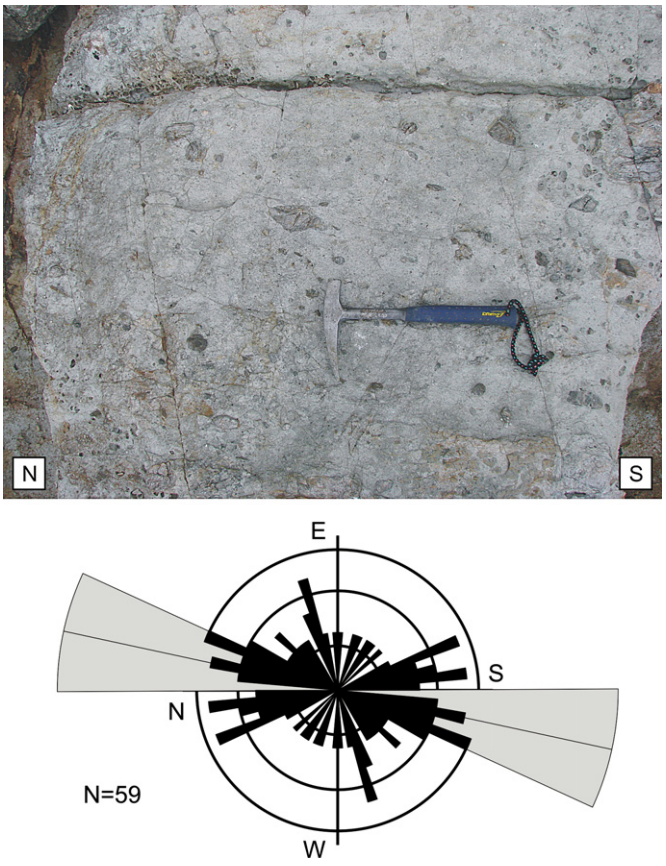

Fig. 6. Photograph of horizontal surface showing an alignment of elongate clasts of quartzite and quartz–mica schist within grey breccia variant C. The clasts are aligned broadly north–south. See Section 4.2 and the caption for Fig. 11 for a description of the construction and labelling of the rose diagram. Orientation statistics were calculated for this example by tracing all visible clasts in the photograph. Mean vector orientation, 12° clockwise from north; mean vector strength, 0.4; mean aspect ratio of visible clasts, 2.17.

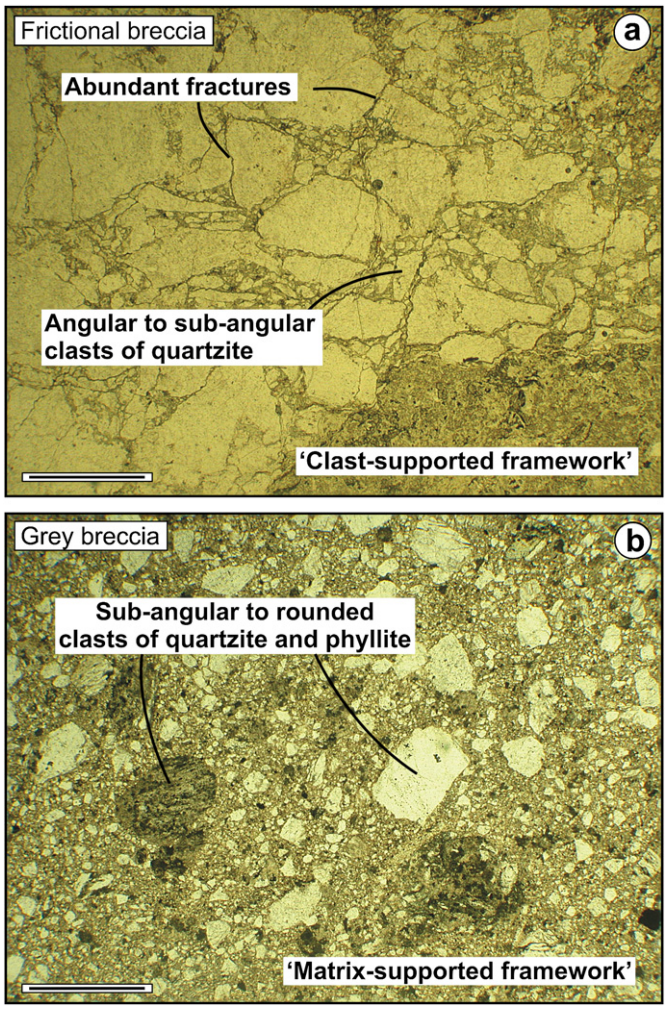

Fig. 7. Photomicrographs showing grain-scale textures within typical frictional breccias (a) and grey breccias (b). Note the 'matrix-supported' framework, and the lack of cataclastic fractures within the grey breccias. Scale bars are 1 mm, and both images are taken in plane polarized light.

4.2. Analysis of clast shape-preferred orientation

Field observations suggest that a mesoscopic shape-preferred orientation (SPO) of quartzite and quartz–mica schist clasts is visible in places within grey breccia variants A and C (Fig. 6). This SPO is aligned roughly north–south on sub-horizontal (plan view) surfaces, but these surfaces only provide a 2-dimensional view of an inherently 3-dimensional SPO vector. To partly overcome this problem, we measured the SPO of clasts within thin sections of grey breccia cut in 3 orthogonal planes through oriented samples collected at the outcrop. Six oriented samples of grey breccia were collected from variants B and C (Fig. 3). Three orthogonal thin sections were cut from each sample, and each thin section is given reference indices to help with identification and analysis. We have followed the labelling convention of Hayman et al. (2004) and provide a description of this convention in the caption for Fig. 11b. Using a BATY® Shadowmaster, thin sections were projected in plane polarized light at ×1 magnification on to a large tracing table. All of the visible clasts within the breccias were traced at ×1 scale. At least 300 clasts were traced in each thin section, although in most cases significantly more than 400 clasts were traced. The resulting images were scanned, processed and imported into ImageTool® textural analysis software (Fig. 10). By tracing all the visible clasts, we eliminate clast selection bias which is usually implicit in manual measurements of SPO at the outcrop or on a grain-scale. Only clasts with an aspect ratio (L/S) greater than 1.5 were included in the final statistical analysis. Although this methodology forces us to restrict our analysis to ×1 magnification, Cladouhos (1999) found that the orientation of the SPO mean vector remains roughly constant at all magnifications.

The results of grain-scale SPO analyses are shown qualitatively as equal-area rose diagrams in Fig. 11b. Quantitatively, the orientation of the mean vector, M, can be calculated using the semi-circular vector mean (Agterberg, 1974; Davis, 2002):

$$M = 0.5\tan^{-1}\left(\frac{\sum \sin 2\theta_i}{\sum \cos 2\theta_i}\right) \quad (2)$$

while the mean vector strength, R, is:

$$R = \frac{1}{N}\left\{\left(\sum \sin 2\theta_i\right)^2 + \left(\sum \cos 2\theta_i\right)^2\right\}^{1/2} \quad (3)$$

for N measurements with clast long axes oriented θ_i. Statistical results for all 6 samples of grey breccia are provided in Table 2.

The results indicate that there is a statistically significant SPO (at a 95% confidence level) of clasts present within the grey breccias. The SPO is strongest in the X1/X2 (horizontal) and X2/X3 (vertical, east–west) sections (Fig. 11b). In the X1/X2 sections, 4 out of 6 samples show a vector strength varying between 0.17 and 0.36. In one sample (Zf002) there is no SPO in the X1/X2 section, and

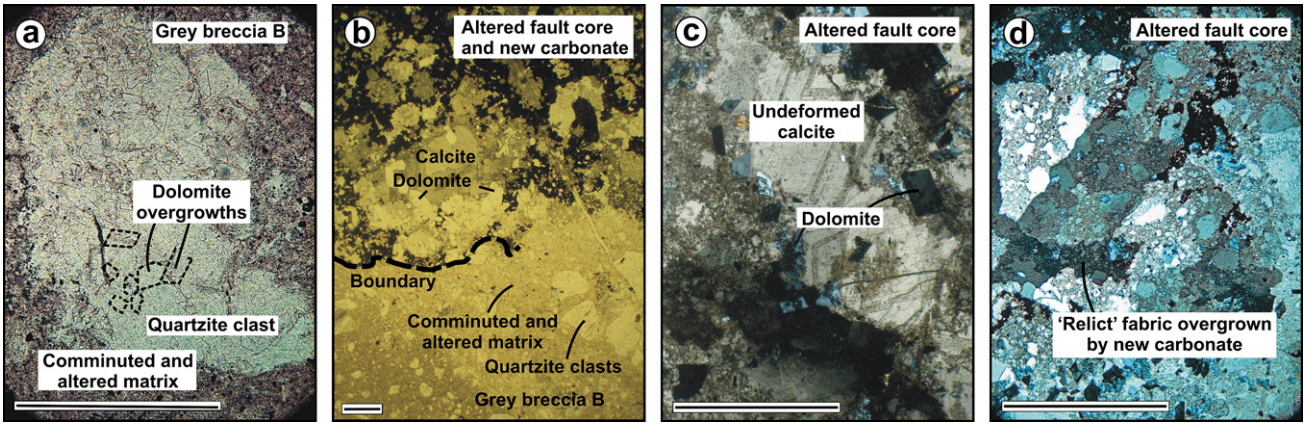

Fig. 8. Photomicrographs showing details of grain-scale textures within grey breccias and overlying fault core. Scale bars are 1 mm. Images (a) and (b) were taken in plane polarized light, (c) and (d) in crossed polarized light. (a) Detail of quartzite clast within grey breccia B which is overgrown by abundant euhedral dolomite crystals. (b) Irregular, well-defined boundary between grey breccia variant B and overlying altered fault rocks within the core of the Zuccale fault. The overlying fault rocks are dominated by fine-grained Fe-oxide phases and fresh growths of calcite and dolomite. (c) Detail of calcite and dolomite intergrowths within altered fault core overlying the boundary. Note the primary growth zoning in both minerals. (d) Relict breccia fabric overgrown by new subhedral–anhedral calcite crystals within the altered fault core.

in another the vector strength is weak (Zf001). For those 4 samples which show a stronger SPO, the orientation of the mean vector is approximately north–south. Significantly, this vector orientation is similar to that observed in horizontal surfaces in the field, suggesting that the grain-scale measurements are reliable. In the X2/X3 sections, all 5 analyses show a vector strength varying between 0.16 and 0.34. One thin section was unsuitable for analysis because the entire slide was occupied by one large clast. All of the mean vector orientations are at a high angle (84–127°) to horizontal. Three out of 6 samples show a significant SPO in the X1/X3 sections (vertical, north–south). However, the vector strengths are generally weak (0.12–0.19) and subordinate to the SPO observed in the other 2 sections. In summary, the dominant shape-preferred orientations of clasts within the grey breccias are approximately north–south in horizontal surfaces, and sub-vertical in east–west trending vertical surfaces.

5. Discussion and conclusions

5.1. Generation of grey breccias

Several outcrop-scale observations suggest that the grey breccias have experienced fluidization. We define fluidization after Monzawa and Otsuki (2003) as "the state in which grains fly around with a mean free path like gaseous molecules". More precisely, we consider fluidization of grey breccias at Punta Di Zuccale to result in the constituent clasts experiencing particle transport in the presence of a fluid phase. First, grey breccias preserve 'intrusive' relationships with foliated fault rocks lying within the core of the Zuccale fault. Second, the boundary between the grey breccias and the fault core is highly irregular and undulose in nature. Third, fragments of altered fault core material are found floating within the underlying grey breccias. Finally, a shape-preferred orientation of clasts is present within all variants of grey breccia. The grey breccias contain low values of fragmented counterparts, providing complementary grain-scale evidence that they experienced fluidization. In addition, the rounded to sub-rounded nature of clasts within the grey breccias has previously been suggested as indicating particle transport in the presence of a fluid (e.g. Clark and James, 2003).

Clasts of quartzite within the grey breccias are commonly overgrown by crystals of dolomite, and the red oxidized layer overlying the grey breccias is dominated by intergrowths of calcite

Table 1
Summary of microstructural observations of typical frictional breccias and grey breccias at Punta Di Zuccale

Frictional breccia	'Clast' supported mosaic texture Abundant cataclastic fractures Matrix is fine grained quartz and fibrous chlorite Upper boundary of breccias is commonly a fault contact Sub-angular to angular clasts
Grey breccia	'Matrix' supported fabric No cataclastic fractures Matrix is ultra-fine grained quartz, sericite, and infrequent chlorite Abundant growth of undeformed calcite and dolomite Quartzite clasts frequently overgrown by dolomite Upper boundary of breccias is intrusive in nature Sub-rounded to rounded clasts

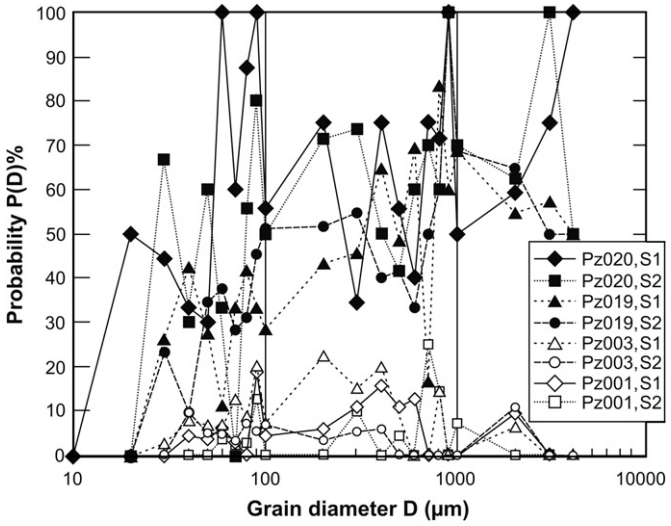

Fig. 9. Detection probability of fragmented counterparts as a function of grain diameter (D) for 4 thin sections of frictional breccia (PZ019, PZ020) and 4 thin sections of grey breccia (PZ001, PZ003). Note the separation in the probability values between the frictional and grey breccias. See text for discussion.

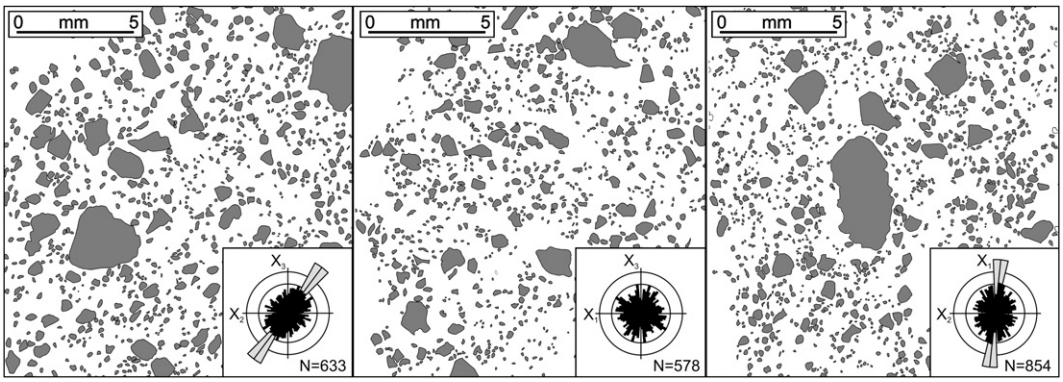

Fig. 10. Examples of images which were used as input to ImageTool® textural analysis software, and the resulting rose diagrams calculated using EZ-ROSE (Baas, 2000). The images represent tracings of 3 thin sections cut along orthogonal planes through one oriented sample. See text for discussion.

and dolomite (Fig. 7). Additionally, there are abundant carbonate hydrofracture veins which cross-cut the footwall and the core of the Zuccale fault. These observations indicate that the fluids which were circulating adjacent to the Zuccale fault contained CO_2. Sources of fluid and CO_2 may include mantle degassing, hydrothermal fluid flow associated with intrusion of the Porto Azzurro pluton, metamorphic fluid, or deeply-circulating meteoric fluid. Regardless of the source(s) of the fluids, recent experimental data (e.g. Le Guen et al., 2007) has shown that CO_2-bearing fluids can cause rapid dissolution of carbonate and silicate minerals, particularly if the fluids are under high partial pressures.

5.1.1. Precursors to fluidization

Grey breccias are developed in the footwall of the Zuccale fault in an area which contains: (a) pre-existing frictional breccias; (b) a north–south trending high-angle footwall fault (Section 3.1); and (c) a strongly foliated fault core dominated by calc-mylonites, phyllonites and foliated cataclasites (Fig. 12a; Section 2.2). Prior to fluidization, the migration of fluids containing CO_2 occurred, which was controlled, at least in part, by fault and fracture networks located in the footwall of the Zuccale fault (Fig. 12a). We suggest that the fluids were forced to pond in structural traps or migrate laterally at the base of the Zuccale fault because of the likely impermeable nature of the foliated fault core (cf. Faulkner and Rutter, 1998, 2000). At this stage, fluids were able to percolate along fracture networks within the pre-existing frictional breccias, causing dissolution of constituent quartzite and quartz–mica schist clasts, and eventually leading to a partial loss of cohesion within the frictional breccias.

5.1.2. Fluidization and the development of fluid overpressures

We interpret the clast-preferred orientations within the grey breccias as representative of a flow fabric generated by fluids moving through the breccias and causing transport and realignment of the constituent clasts. The SPO data are consistent with fluids moving upwards within the footwall from depth and spreading laterally in a north–south direction once they encountered the relatively impermeable fault core. This scenario would account for the sub-vertical SPO observed on vertical planes and the approximately north–south SPO observed on horizontal planes.

All major hydrofracture veins which cross-cut the fault core link directly downwards into high-angle footwall faults, strongly suggesting that footwall structures act to focus and channel fluid flow (Section 2.2, Fig. 2). We believe that the SPO of clasts within the grey breccias can be explained by invoking fluidization during periodic slip events along high-angle footwall faults (Fig. 12b). During such slip events, fault planes can experience dilation allowing short-term focused fluid flow at rates of up to several 10s of centimetres per second (Sibson, 2000; Eichhubl and Boles, 2000; Sheldon and Ord, 2005). The overlying fault core in this case maintained its integrity, and its low permeability, by continuing to experience macroscopically ductile deformation, meaning that the footwall-hosted fluid pulse was forced to spread laterally beneath the core, explaining the development of an SPO on horizontal (plan view) surfaces (Fig. 12b). This scenario also satisfies a condition of Bagnold's (1954) experimental investigation into the generation of fluidized granular materials. He showed that the transition from frictional deformation to fluidization occurs when the Bagnold number decreases from infinity to a finite value (larger than 450), and that the most likely reason for this is a small decrease in the volume fraction of clasts. To explain this small decrease, Monzawa and Otsuki (2003) and Otsuki et al. (2003) invoked normal interface vibration (Brune et al., 1993) and a resulting increase in the distance between fault wall rocks. In our model, a small decrease in the volume fraction of breccia clasts beneath the Zuccale fault could result directly from slip along high-angle footwall faults in one of two ways: (1) fault plane dilation; or (2) the hangingwall of such faults would experience negative (tensional) static stress changes

Table 2
Shape-preferred orientation statistics for 6 samples (18 thin sections) of grey breccia (see Fig. 11 for corresponding rose diagrams and orientation conventions)

Sample	X2X3				X1X3				X1X2			
	M	*R*	*L/S*	*N*	*M*	*R*	*L/S*	*N*	*M*	*R*	*L/S*	*N*
Zf001 (C)	97.08	0.19	2.04	622	17.73	0.16	1.92	684	30.6	0.08	1.89	836
Zf002 (B)	126	0.34	1.8	422			1.67	531			1.7	531
Zf003 (B)	84.35	0.16	1.84	469			1.89	476	107.6	0.19	1.84	620
Zf004 (C)	126.61	0.2	1.85	633			1.86	578	95.91	0.17	1.85	854
Zf005 (C)	89.392	0.181	1.82	555	34.64	0.12	1.70	324	80.48	0.358	1.84	396
Zf006 (C)					40.1	0.19	1.78	516	102.39	0.239	2.02	400

M, mean vector orientation (α°); *R*, mean vector strength; *L/S*, mean aspect ratio; *N*, number of clasts used in each thin section. Boxes are left blank where results were not statistically significant at 95% confidence.

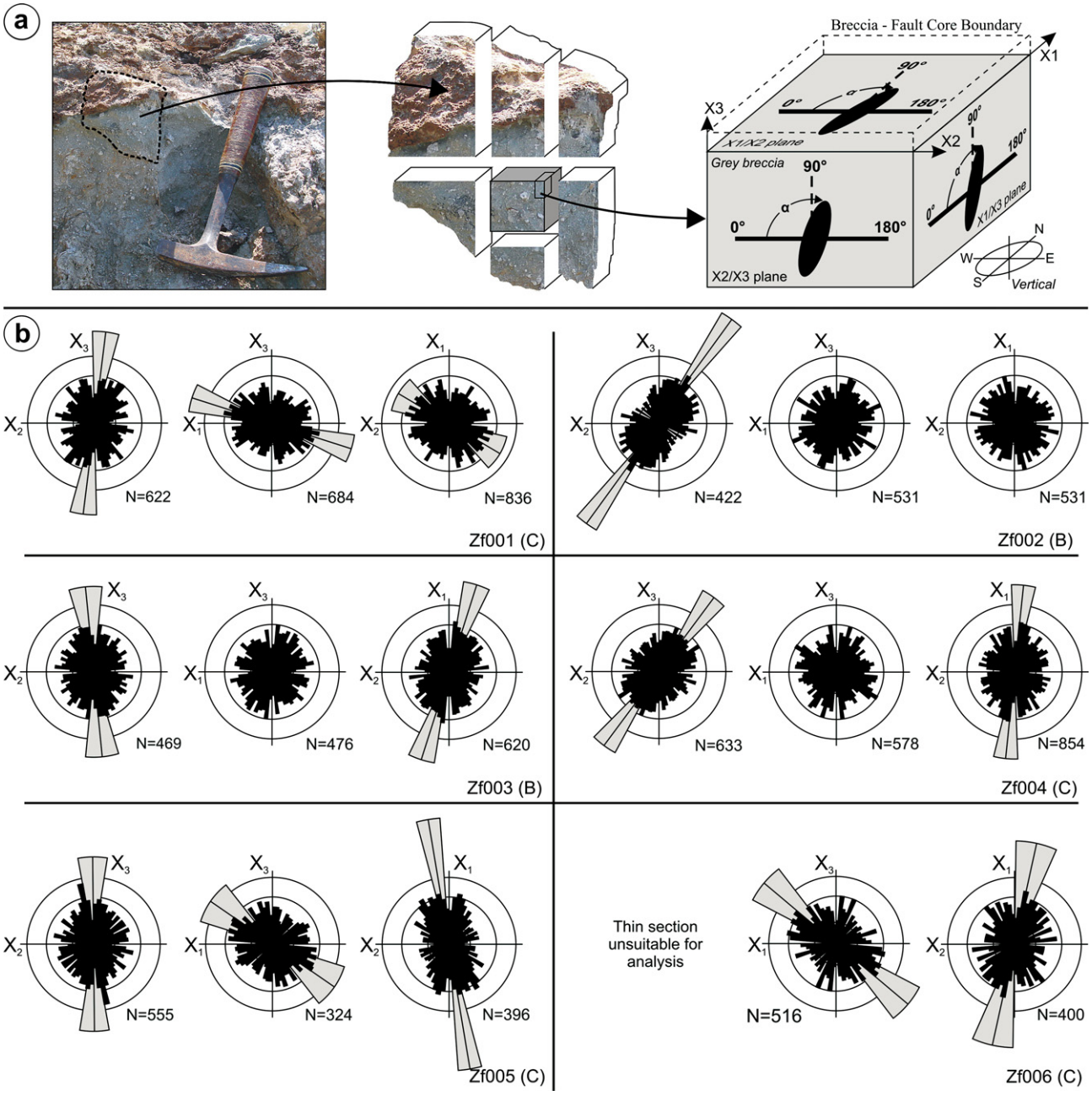

Fig. 11. (a) Orientation conventions used for calculating grain-scale shape-preferred orientation (SPO). Three orthogonal thin sections were cut from samples collected in the field. The X1/X2 thin section is sub-horizontal, and the edges of the thin section aligned with X1 (north–south) and X2 (east–west). The X2/X3 thin section is vertical, and the edges of the thin section aligned with X2 and X3. The X1/X3 thin section is vertical, and the edges of the thin section aligned with X1 and X3. α is the angle (0–180° measured clockwise) between the reference line indicated and the long-axis of the measured clast. (b) Equal-area rose diagrams of the shape-preferred orientation of clasts within 6 samples of grey breccia (Zf001–Zf006; letters in brackets refer to the grey breccia variant from which the sample was taken). The rose diagrams were constructed using EZ-ROSE (Baas, 2000) and the data are plotted in 5° bin intervals. The outer circle represents 10% of the data. The grey sector in each rose diagram shows the mean vector orientation (black bisector line) and mean vector strength (length of grey sector). The angular confidence interval (95% confidence) is indicated by the width of the grey sector. *N* is the total number of clasts measured in each thin section. In all cases $N > 300$, usually $N \gg 400$. Where no grey sector is present, the data has a uniform distribution and there is no statistically significant preferred orientation at 95% confidence. Measurements of all angles presented in Table 2 are clockwise from the reference line indicated in part (a). One thin section from sample Zf006 was unsuitable for microscopic analysis.

(Nostro et al., 1997). The most likely reason for approximately north–south directed lateral flow beneath the fault core is enhanced permeability parallel to the σ_2 direction and the strike of the footwall fault (e.g. Sibson, 2000).

The ponding of fluids at the base of the Zuccale fault as a consequence of a waning in flow could result in the slow growth of fresh and undeformed carbonate within a thin alteration horizon overlying the grey breccias (Figs. 4, 12b). This may also explain the fact that large clasts of quartzite and quartz–mica schist, now eroded to form a honeycomb texture, appear to have settled downwards towards the base of breccia variant C (Fig. 5b). During successive slip events along the high-angle footwall fault, continued input of fluids would lead to a gradual increase in the concentration of CO_2, eventually leading to gas bubble formation. This would increase fluid overpressure, inducing deformation (warping and folding) of the boundary between the grey breccias and the

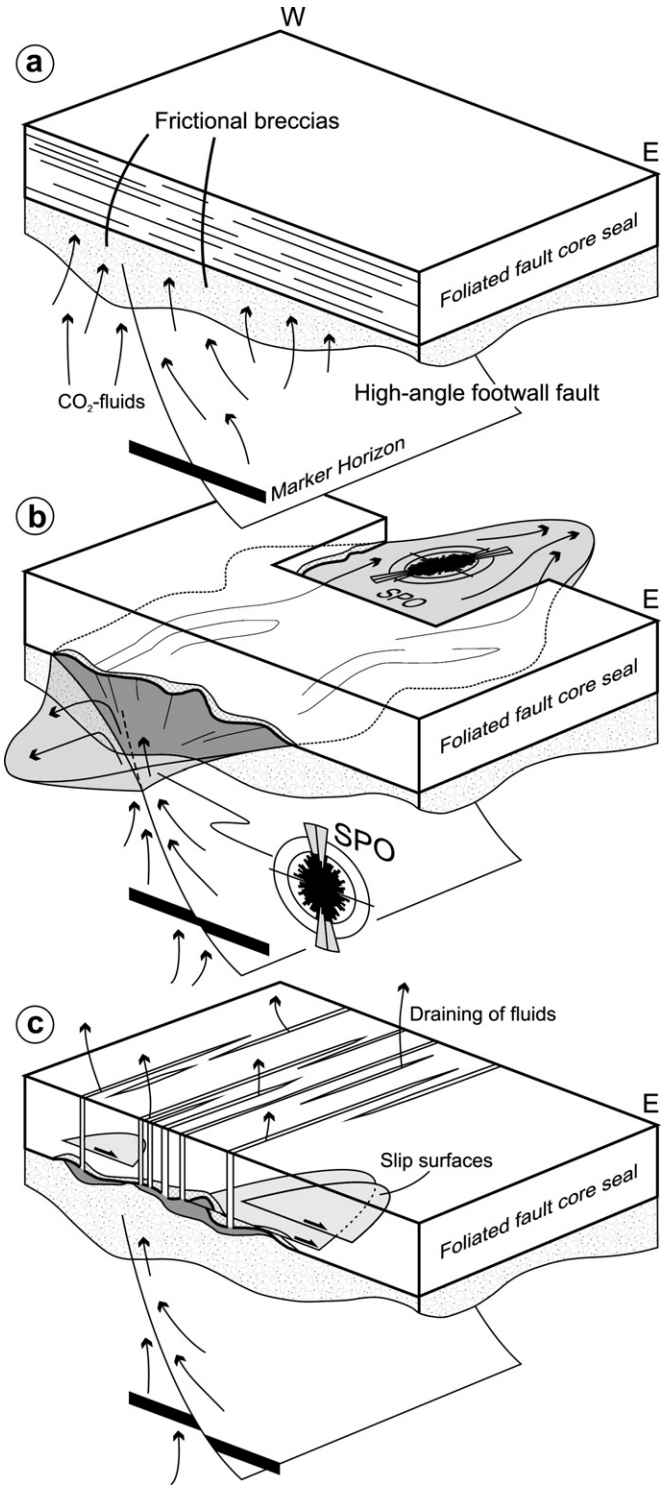

Fig. 12. Generation of grey breccias. (a) Precursors to fluidization: the Zuccale fault possesses a strongly foliated fault core which acts as a low-permeability seal to CO_2-bearing fluids migrating within the footwall. The fault core is underlain by a high-angle footwall fault. Fluids infiltrate pre-existing frictional breccias, leading to dissolution and a loss of cohesion. (b) Fluidization: periodic slip along high-angle footwall faults leads to focused and rapid fluid flow, causing fluidization of clasts within the frictional breccias. The fluid pulse spreads laterally as it encounters the fault core. Ponding of fluids, and deformation of the boundary, may occur during continued input of fluids. (c) Hydrofracturing: critical fluid overpressure leads to embrittlement within the core of the Zuccale fault, allowing fluids to drain from footwall to hangingwall. The fractures undergo healing processes returning to a low-permeability nature, allowing the fault-valve cycle to repeat.

fault core, and promoting the incorporation of fault core material into the breccias (Figs. 4, 5). Deformation of the boundary may also have been enhanced by reaction-weakening processes within the fault core, triggered by the presence of chemically active CO_2-bearing fluids.

5.1.3. Hydrofracturing and fault-valve behaviour

Once fluid overpressure in the footwall of the Zuccale fault reached a critical value (e.g. $P_f = \sigma_3 + T$), this triggered hydrofracturing of the fault core and a significant increase in permeability, allowing fluids to drain from the footwall into the hangingwall (Fig. 12c). We speculate that an increase in fluid overpressure also promoted movement along extensional slip surfaces within the fault core, because at Punta Di Zuccale, the concentration of these slip surfaces is greatest within the fault core immediately overlying the grey breccias. As described in Section 3.1, grey breccia variant A is cross-cut along its upper margin by a low-angle slip surface. Draining of fluids from the footwall to the hangingwall resulted in a decrease in fluid overpressure. Hydrofractures and slip surfaces were mineralized, and the fault core underwent sealing processes returning to a low-permeability state (e.g. Tenthorey and Cox, 2006; Gratier and Gueydan, 2007). The presence of multiple variants of grey breccia attests to the fact that fluid flow along the Zuccale fault was cyclic. The combined grey breccia–hydrofracture–slip surface association therefore represents an integrated example of fault-valve behaviour along low-angle normal faults.

5.2. Fluidized fault rocks and the seismic cycle

Fluidized fault rocks have been described on several occasions in the literature from a variety of tectonic settings. These include, but are not restricted to: decimetre-thick lenses of fluidized cataclasite found in association with pseudotachylytes within ancient accretionary complexes (Rowe et al., 2005; Ujiie et al., 2007); centimetre-thick fluidized cataclasites and fault gouges from major intracontinental strike-slip faults in Japan (Monzawa and Otsuki, 2003; Otsuki et al., 2003); fluidized breccias found as meter-scale dyke- and pipe-like bodies around intrusions, faults and near ore deposits in eastern Australia (Oliver et al., 2006) and South Africa (Boorman et al., 2003); and variably-sized fluidized breccias controlled by dilational fault jogs (e.g. Clark and James, 2003). In each of these cases, the fluidized fault rocks are found as bodies which cross-cut wall rocks with sharp angular contacts, and are interpreted as forming due to single rapid events related to a sudden release, or increase, of fluid overpressure. The close link between fluidized cataclasites and pseudotachylytes found along exhumed subduction thrust faults prompted Rowe et al. (2005) and Ujiie et al. (2007) to suggest that this type of fluidized cataclasite may be used as an indicator of co-seismic slip.

We believe that fluidization of the grey breccias found at Punta Di Zuccale is related to the interactions between slip along the low-angle Zuccale fault (which accommodates 6–8 km of displacement), and slip along high-angle footwall faults (individually accommodating, at most, 5 m of displacement). With respect to the Zuccale fault, we suggest that fluidization of the grey breccias is related to gradual build-ups of fluid overpressure in the footwall of the Zuccale fault during the interseismic stage of the earthquake cycle. It is important to note that build-ups of fluid overpressure were punctuated by co-seismic slip events along high-angle footwall faults, but not by slip events within the low-angle core of the Zuccale fault itself. In other words, the fault-valve and seismic-cycle along the Zuccale fault were intimately related to, and dependent upon, the fault-valve and seismic cycle along the high-angle footwall faults.

During the interseismic stage along the Zuccale fault, the fault core likely possessed a low permeability and was deforming by mechanisms such as pressure-solution ('frictional-viscous') creep (Bos and Spiers, 2002; Collettini and Holdsworth, 2004). Migration of CO_2-bearing fluids at this stage acted to corrode frictional breccias in the footwall. Both migration of fluids and corrosion of frictional breccias were essential precursors to fluidization. Build-ups of fluid overpressure in the footwall of the Zuccale fault, perhaps combined with reaction weakening within the fault core, led to deformation and folding of the boundary between the grey breccias and the fault core. Only when fluid overpressure in the footwall obtained a critical value could hydrofracturing and brittle slip occur along the Zuccale fault. In our opinion, the size of the grey breccias, characteristics of the boundary with the overlying Zuccale fault core, and structural position *beneath* the fault core, are most compatible with fluidization having occurred during the interseismic period along the Zuccale fault. Comparison with the studies of fluidized fault rocks mentioned above suggests that fluidization of grey breccias during co-seismic slip along the Zuccale fault would have resulted in angular and sharp cross-cutting relationships with the fault core and local wall rocks, and/or formation of fluidized material formed by slip *within*, and emanating from, the core of the Zuccale fault.

The fluidization of grey breccias at Punta Di Zuccale occurred over areas of 10^{-3}–10^{-2} km^2. We suggested in Section 5.1.3, based on field evidence, that attainment of critical fluid overpressures in the footwall of the Zuccale fault triggered the formation of low-angle extensional slip surfaces within the overlying fault core, and therefore it seems likely that the slip surfaces would possess dimensions roughly equal to those of the grey breccias. We speculate that hydrofracturing and brittle slip processes, triggered by fluid overpressure, may represent co-seismic events along the low-angle Zuccale fault. Interestingly, microseismicity produced along the active Altotiberina low-angle normal fault occurs on rupture surfaces on the order of 10^{-3}–10^{-1} km^2.

Cowan (1999) concluded that, based on our current understanding, the only fault rocks which are unambiguous indicators of co-seismic slip are pseudotachylytes. More recently, Han et al. (2007a,b) conducted high-velocity friction experiments and reported that at seismic slip velocities (up to 2 m s^{-1}) calcite and siderite experienced thermal decomposition resulting in formation of CO_2 + lime and CO_2 + magnetite, respectively. Ujiie et al. (2008) also suggested that stretching of fluid inclusions in calcite might indicate frictional heating associated with co-seismic slip. The present study shows that it is possible to identify distinctive fault rocks and fault structures which are characteristic of different parts of the seismic cycle. In order to do this, it is necessary to document geological evidence that constrains the likely fluctuations in fluid pressure that occur as well as the ways in which different parts of the overall fault network (e.g. low-angle fault core and high-angle footwall faults) may mutually interact through time. Ultimately this will lead to important advances in fault and earthquake mechanics, particularly along enigmatic structures such as low-angle normal faults.

Acknowledgements

S.A.F.S. is funded by a University of Durham Doctoral Fellowship. Fieldwork was supported by grants from The Geological Society of London, the American Association of Petroleum Geologists, the Geologists Association, the Mineralogical Society of Great Britain and Ireland, the Edinburgh Geological Society, and the John Ray Trust. Discussions with Nicola De Paola, and comments from Tom Blenkinsop, proved very helpful. Dougal Jerram provided useful advice on using ImageTool® software. Nick Oliver and an anonymous reviewer are thanked for helping us to clarify our arguments and significantly improve the quality of the manuscript. Tom Blenkinsop is also thanked for his editorial handling of the manuscript.

References

Agterberg, F.P., 1974. Geomathematics: Mathematical Background and Geoscience Applications. Elsevier, Amsterdam.
Anderson, E.M., 1942. The Dynamics of Faulting and Dyke Formation with Application to Britain. Oliver & Boyd, Edinburgh.
Axen, G.J., 2004. Mechanics of low-angle normal faults. In: Karner, G.D., Morris, J.D., Driscoll, N.W., Silver, E.A. (Eds.), Rheology and Deformation of the Lithosphere at Continental MarginsMARGINS Theoretical and Experimental Earth Science Series, Chapter 3. Columbia University Press, pp. 46–91.
Axen, G.J., 2007. Research focus: significance of large-displacement, low-angle normal faults. Geology 35, 287–288.
Baas, J.H., 2000. EZ-ROSE: a computer program for equal-area circular histograms and statistical analysis of two-dimensional vectorial data. Computers & Geosciences 26, 153–166.
Bagnold, R.A., 1954. Experiments on a gravity-free dispersion of large solid spheres in a Newtonian fluid under shear. Proceedings of the Royal Society London, Series A 225, 49–63.
Barchi, M.R., Minelli, G., Pialli, G., 1998. The CROP 03 profile: a synthesis of results on deep structures of the Northern Apennines. Memorie della Societa Geologica Italiana 52, 383–400.
Boncio, P., Brozetti, F., Ponziani, F., Barchi, R.M., Lavecchia, G., Pialli, G., 1998. Seismicity and extensional tectonics in the northern Umbria-Marches Apennines. Memorie della Societa Geologica Italiana 52, 539–555.
Boncio, P., Brozetti, F., Lavecchia, G., 2000. Architecture and seismotectonics of a regional low-angle normal fault in central Italy. Tectonics 19, 1038–1055.
Boorman, S.J., McGuire, J.B., Boudreau, A.E., Kruger, F.J., 2003. Fluid overpressure in layered intrusions: formation of a breccia pipe in the eastern Bushveld Complex, Republic of South Africa. Mineralium Deposita 38, 356–369.
Bortolotti, V., Fazzuoli, M., Pandeli, E., Principi, G., Babbini, A., Corti, S., 2001. Geology of central and Eastern Elba island, Italy. Ofioliti 26, 97–150.
Bos, B., Spiers, C.J., 2002. Frictional-viscous flow of phyllosilicate-bearing fault rock: microphysical model and implications for crustal strength profiles. Journal of Geophysical Research 107 (B), 2028, doi:10.1029/2001JB000301.
Brune, J.N., Brown, S., Johnson, P.A., 1993. Rupture mechanism and interface separation in foam rubber models of earthquakes: a possible solution to the heat flow paradox and the paradox of large overthrusts. In: Tectonophysics, 218 59–67.
Chiaraluce, L., Chiarabba, C., Collettini, C., Piccinini, D., Cocco, M., 2007. The architecture and mechanics of an active low angle normal fault: the Alto Tiberina Fault, northern Apennines, Italy. Journal of Geophysical Research 112, doi:10.1029/2007JB005015 B10310.
Chiodini, G., Cioni, R., 1989. Gas geobarometry for hydrothermal systems and its application to various Italian geothermal areas. Applied Geochemistry 4, 465–472.
Chiodini, G., Cardellini, C., Amato, A., Boschi, E., Caliro, S., Frondini, F., Ventura, G., 2004. Carbon dioxide Earth degassing and seismogenesis in central and southern Italy. Geophysical Research Letters 31, doi:10.1029/2004GL019480 L07615.
Cladouhos, T.T., 1999. Shape-preferred orientations of survivor grains in fault gouge. Journal of Structural Geology 21, 419–436.
Clark, C., James, P., 2003. Hydrothermal brecciation due to fluid pressure fluctuations: examples from the Olary Domain, South Australia. Tectonophysics 366, 187–206.
Collettini, C., Barchi, M.R., 2002. A low-angle normal fault in the Umbria region (central Italy): a mechanical model for the related microseismicity. Tectonophysics 359, 97–115.
Collettini, C., Holdsworth, R.E., 2004. Fault zone weakening processes along low-angle normal faults: insights from the Zuccale fault, Isle of Elba, Italy. Journal of the Geological Society 161, 1039–1051.
Collettini, C., Sibson, R.H., 2001. Normal faults, normal friction? Geology 29, 927–930.
Collettini, C., De Paola, N., Goulty, N.R., 2006a. Switches in the minimum compressive stress direction induced by overpressure beneath a low-permeability fault zone. Terra Nova 18, 224–231.
Collettini, C., De Paola, N., Holdsworth, R.E., Barchi, M.R., 2006b. The development and behavior of low-angle normal faults during Cenozoic asymmetric extension in the Northern Apennines, Italy. Journal of Structural Geology 28, 333–352.
Cowan, D.S., 1999. Do faults preserve a record of seismic slip? A field geologists opinion. Journal of Structural Geology 21, 995–1001.
Cox, S.F., 1995. Faulting processes at high fluid pressures: an example of fault-valve behavior from the Wattle Gully Fault, Victoria, Australia. Journal of Geophysical Research 100, 12841–12859.
Davis, J.C., 2002. Statistics and Data Analysis in Geology, third ed. John Wiley & Sons.
Dini, A., Innocenti, F., Rocchi, S., Tonarini, S., Westerman, D.S., 2002. The magmatic evolution of the late Miocene laccolith–pluton–dyke granitic complex of Elba Island, Italy. Geological Magazine 139, 257–279.
Elter, P., Giglia, G., Tongiorgi, M., Trevisan, L., 1975. Tensional and contractional areas in recent Tortonian to present evolution of the Northern Apennines. Bollettino di Geofisica Teorica ed Applicata 17, 1975.
Eichhubl, P., Boles, J.R., 2000. Rates of fluid flow in fault systems – evidence for episodic rapid fluid flow in the Miocene Monterey Formation, coastal California. American Journal of Science 300, 571–600.

Famin, V., Hebert, R., Philippot, P., Jolivet, L., 2005. Ion probe and fluid inclusion evidence for co-seismic fluid infiltration in a crustal detachment. Contributions to Mineralogy and Petrology 150, 354–367.

Faulkner, D.R., Rutter, E.H., 1998. The gas permeability of clay-bearing fault gouge at 20 °C. In: Jones, G., Fisher, Q.J., Knipe, R.J. (Eds.), Faulting, Fault Sealing and Fluid Flow in Hydrocarbon Reservoirs. Special Publications, vol. 147. Geological Society, London, pp. 147–156.

Faulkner, D.R., Rutter, E.H., 2000. Comparisons of water and argon permeability in natural clay-bearing fault gouge under high-pressure at 20 °C. Journal of Geophysical Research 105 (B7), 16415–16426.

Gagnevin, D., Daly, J.S., Poli, G., 2004. Petrographic, geochemical and isotopic constraints on magma dynamics and mixing in the Miocene Monte Capanne monzogranite (Elba Island, Italy). Lithos 78, 157–195.

Gratier, J.P., Gueydan, F., 2007. Deformation in the presence of fluids and mineral reactions: effects of fracturing and fluid-rock interaction on seismic cycles. In: Handy, M.R., Hirth, G., Hovius, N. (Eds.), Tectonic Faults: Agents of Change on a Dynamic Earth, Dahlem Workshop Reports. The MIT Press, pp. 319–356.

Han, R., Shimamoto, T., Ando, J., Ree, J.H., 2007a. Seismic slip record in carbonate-bearing fault zones: an insight from high-velocity friction experiments on siderite gouge. Geology 35, 1131–1134.

Han, R., Shimamoto, T., Hirose, T., Ree, J.H., Ando, J., 2007b. Ultralow friction of carbonate faults caused by thermal decomposition. Science 316, 878–881.

Hayman, N.W., Housen, B.A., Cladouhos, T.T., Livi, K., 2004. Magnetic and clast fabrics as measurements of grain-scale processes within the Death Valley shallow crustal detachment faults. Journal of Geophysical Research 109, doi:10.1029/2003JB002902 B05409.

Henderson, I.H.C., McCaig, A.M., 1996. Fluid pressure and salinity variations in shear zone related veins, central Pyrenees, France: implications for the fault-valve model. Tectonophysics 262, 321–348.

Hickman, S., Sibson, R.H., Bruhn, R., 1995. Introduction to special section: Mechanical involvement of fluids in faulting. Journal of Geophysical Research 100, 12831–12840.

Jackson, J.A., White, N.J., 1989. Normal faulting in the upper continental crust: observations from regions of active extension. Journal of Structural Geology 11, 15–36.

Jolivet, L., Faccannena, C., Goffe, B., Mattei, M., Rossetti, F., Brunet, C., Storti, F., Funiciello, R., Cadet, J.P., D'Agostino, N., Parra, T., 1998. Midcrustal shear zones in postorogenic extension: examples from the northern Tyrrhenian Sea. Journal of Geophysical Research 103, 12123–12160.

Keller, J.V.A., Pialli, G., 1990. Tectonics of the island of Elba: a reappraisal. Bollettino della Societa Geologica Italiana 109, 413–425.

Keller, J.V.A., Coward, M.P., 1996. The structure and evolution of the northern Tyrrhenian Sea. Geological Magazine 133, 1–16.

Le Guen, Y., Renard, F., Hellmann, R., Brosse, E., Collombet, M., Tisserand, D., Gratier, J.P., 2007. Enhanced deformation of limestone and sandstone in the presence of high PCO_2 fluids. Journal of Geophysical Research 112, doi:10.1029/2006JB004637.

Maineri, C., Benvenuti, M., Costaglioli, P., Dini, A., Lattanzi, P., Ruggieri, G., Villa, I.M., 2003. Sericitic alteration at the La Crocceta deposit (Elba Island, Italy): interplay between magmatism, tectonics and hydrothermal activity. Mineralium Deposita 38, 67–86.

Miller, S.A., Collettini, C., Chiaraluce, L., Cocco, M., Barchi, M.R., Kaus, B., 2004. Aftershocks driven by a high pressure CO_2 source at depth. Nature 427, 724–727.

Minissale, A., 2004. Origin, transport and discharge of CO_2 in central Italy. Earth-Science Reviews 66, 89–141.

Minissale, A., Magro, G., Martinelli, G., Vaselli, O., Tassi, G.F., 2000. Fluid geochemical transect in the Northern Apennines (central-northern Italy): fluid genesis and migration and tectonic implications. Tectonophysics 319, 199–222.

Montone, P., Mariucci, M.T., Pondrelli, S., Amato, A., 2004. An improved stress map for Italy and surrounding regions (central Mediterranean). Journal of Geophysical Research 109, doi:10.1029/2003JB002703 B10410.

Monzawa, N., Otsuki, K., 2003. Comminution and fluidization of granular fault materials: implications for fault slip behaviour. Tectonophysics 367, 127–143.

Mort, K., Woodcock, N.H., 2008. Quantifying fault breccia geometry: Dent Fault, NW England. Journal of Structural Geology, doi:10.1016/j.jsg.2008.02.005.

Nguyen, P.T., Cox, S.F., Harris, L.B., Powell, C.M., 1998. Fault-valve behavior in optimally oriented shear zones: an example at Revenge gold mine, Kambalda, Western Australia. Journal of Structural Geology 20, 1625–1640.

Nostro, C., Cocco, M., Belardinelli, M.E., 1997. Static stress changes in extensional regimes: an application to southern Apennines (Italy). Bulletin of the Seismological Society of America 87, 234–248.

Numelin, T., Marone, C., Kirby, E., 2007. Frictional properties of natural fault gouge from a low-angle normal fault, Panamint Valley, California. Tectonics 26, doi:10.1029/2005TC001916 TC2004.

Oliver, N.H.S., 1996. Review and classification of structural controls on fluid flow during regional metamorphism. Journal of Metamorphic Geology 14, 477–492.

Oliver, N.H.S., Rubenach, M.J., Fu, B., Baker, T., Blenkinsop, T.G., Cleverley, J.S., Marshall, L.J., Ridd, P.J., 2006. Granite-related overpressure and volatile release in the mid-crust: fluidized breccias from the Cloncurry district, Australia. Geofluids 6, 346–358.

Otsuki, K., Monzawa, N., Nagase, T., 2003. Fluidization and melting of fault gouge during seismic slip: identification in the Nojima fault zone and implications for focal earthquake mechanisms. Journal of Geophysical Research 108 (B4), doi:10.1029/2001JB001711 2192.

Parry, W.T., Bruhn, R.L., 1990. Fluid pressure transients on seismogenic normal faults. Tectonophysics 179, 335–344.

Pascucci, V., Merlini, S., Martini, I.P., 1999. Seismic stratigraphy in the Miocene-Pleistocene sedimentary basins of the Northern Tyrrhenian Sea and western Tuscany (Italy). Basin Research 11, 337–356.

Pauselli, C., Federico, C., 2002. The brittle/ductile transition along the CROP03 seismic profile: relationship with the geological features. Bollettino della Societa Geologica Italiana 1, 25–35.

Pauselli, C., Barchi, M.R., Federico, C., Magnani, M.B., Minelli, G., 2006. The crustal structure of the northern Apennines (Central Italy): an insight by the CROP03 seismic line. American Journal of Science 306, 428–450.

Person, M., Baumgartner, L.P., Bos, B., Connolly, J.A.D., Gratier, J.P., Gueydan, F., Miller, S.A., Rosenberg, C.L., Urai, J.L., Yardley, B., 2007. Group report: Fluids, geochemical cycles, and mass transport in fault zones. In: Handy, M.R., Hirth, G., Hovius, N. (Eds.), Tectonic Faults: Agents of Change on a Dynamic Earth. The MIT Press, pp. 403–425. Dahlem Workshop Reports.

Reynolds, S.J., Lister, G.S., 1987. Structural aspects of fluid–rock interactions in detachment zones. Geology 15, 362–366.

Rossetti, F., Tecce, F., Billi, A., Brilli, M., 2007. Patterns of fluid flow in the contact aureole of the Late Miocene Monte Capanne pluton (Elba Island, Italy): the role of structures and rheology. Contributions to Mineralogy and Petrology 153, 743–760.

Rowe, C.D., Moore, J.C., Meneghini, F., McKeirnan, A.W., 2005. Large-scale pseudotachylytes and fluidized cataclasites from an ancient subduction thrust fault. Geology 33, 937–940.

Sheldon, H.A., Ord, A., 2005. Evolution of porosity, permeability and fluid pressure in dilatant faults post-failure: implications for fluid flow and mineralization. Geofluids 5, 272–288.

Sibson, R.H., 1989. Earthquake faulting as a structural process. Journal of Structural Geology 11, 1–14.

Sibson, R.H., 1990. Conditions for fault-valve behavior. In: Knipe, R.J., Rutter, E.H. (Eds.), Deformation Mechanisms, Rheology and Tectonics. Special Publications, vol. 54. Geological Society, London, pp. 15–28.

Sibson, R.H., 1992. Implications of fault-valve behavior for rupture nucleation and recurrence. Tectonophysics 18, 1031–1042.

Sibson, R.H., 2000. Fluid involvement in normal faulting. Journal of Geodynamics 29, 469–499.

Sibson, R.H., 2007. An episode of fault-valve behavior during compressional inversion? The 2004 M(J)6.8 Mid-Niigata Prefecture, Japan, earthquake sequence. Earth and Planetary Science Letters 257, 188–199.

Smith, S.A.F., Holdsworth, R.E., Collettini, C., Imber, J., 2007. Using footwall structures to constrain the evolution of low-angle normal faults. Journal of the Geological Society London 164, 1187–1191.

Taylor, H.P., Turi, B., 1979. High-^{18}O igneous rocks from the Tuscan magmatic province, Italy. Contributions to Mineralogy and Petrology 55, 33–54.

Tenthorey, E., Cox, S.F., 2006. Cohesive strengthening of fault zones during the interseismic period: an experimental study. Journal of Geophysical Research, Solid Earth 111 (B9) B09202.

Trevisan, L., Marinelli, G., Barberi, F., Giglia, G., Innocenti, F., Raggi, G., Squarci, P., Taffi, L., Ricci, C.A., 1967. Carta Geologica dell'Isola d'Elba. Scala 1:25.000. Consiglio Nazionale delle Ricerche, Gruppo di Ricerca per la Geologia dell'Appennino centro-settentrionale e della Toscana. Pisa, Italy.

Ujiie, K., Yamaguchi, A., Kimura, G., Toh, S., 2007. Fluidization of granular material in a subduction thrust at seismogenic depths. Earth and Planetary Science Letters 259, 307–318.

Ujiie, K., Yamaguchi, A., Taguchi, S., 2008. Stretching of fluid inclusions in calcite as an indicator of frictional heating on faults. Geology 36, 111–114.

Wernicke, B., 1995. Low-angle normal faults and seismicity: a review. Journal of Geophysical Research 100, 20159–20174.